Electron temperature measurement by a helium line intensity ratio method in helicon plasmas

R. F. Boivin, J. L. Kline, and E. E. Scime
Department of Physics, West Virginia University, Morgantown, West Virginia 26506

(Received 14 June 2001; accepted 19 September 2001)

Electron temperature measurements in helicon plasmas are difficult. The presence of intense rf fields in the plasma complicates the interpretation of Langmuir probe measurements. Furthermore, the non-negligible ion temperature in the plasma considerably shortens the lifetime of conventional Langmuir probes. A spectroscopic technique based on the relative intensities of neutral helium lines is used to measure the electron temperature in the HELIX (Hot hELicon eXperiment) plasma [P. A. Keiter *et al.*, Phys. Plasmas **4**, 2741 (1997)]. This nonintrusive diagnostic is based on the fact that electron impact excitation rate coefficients for helium singlet and triplet states differ as a function of the electron temperature. The different aspects related to the validity of this technique to measure the electron temperature in rf generated plasmas are discussed in this paper. At low plasma density ($n_e \leqslant 10^{11}\,\mathrm{cm}^{-3}$), this diagnostic is believed to be very reliable since the population of the emitting level can be easily estimated with reasonable accuracy by assuming that all excitation originates from the ground state (steady-state corona model). At higher density, secondary processes (excitation transfer, excitation from metastable, cascading) become more important and a more complex collisional radiative model must be used to predict the electron temperature. In this work, different helium transitions are examined and a suitable transition pair is identified. For an electron temperature of 10 eV, the line ratio is measured as a function of plasma density and compared to values predicted by models. The measured line ratio function is in good agreement with theory and the data suggest that the excitation transfer is the dominant secondary process in high-density plasmas. © *2001 American Institute of Physics.* [DOI: 10.1063/1.1418020]

I. INTRODUCTION

The measurement of electron temperature in helicon plasma sources is a complicated venture. The presence of intense rf fields in the plasma complicates the interpretation of conventional Langmuir probe measurements.[1,2] Lately, the introduction of an rf compensated probe[3] has provided a satisfactory means of measuring T_e. However, to obtain the complete characteristic $I-V$ curve, one must still bias the probe to a large negative potential. This biasing process combined with the non-negligible ion temperature observed in helicon plasmas[4] will sputter material from the probe tip and contaminate the plasma. This sputtering process will be especially strong in high-density plasmas and will lead to many interpretation problems associated with the contamination (re-deposition) and erosion of probe tips exposed to ion bombardment (reduction of the diameter, augmentation of the total exterior surface of the probe). Hence, continuous plasma exposure progressively reduces the precision of the probe, shortens its useful lifetime, and increases the odds of catastrophic failure.

Measuring plasma parameters with noninvasive diagnostics is also preferred in many applications where rf sources are used. For example, plasma processing or plasma-assisted systems are often used to generate reactive species for film growth. In these systems, a small concentration of metallic or reactive impurities can lead to the formation of point defects in the lattice, which results in poor electrical quality films.[5] Another possible application of nonintrusive diagnostics is within the plasma thruster concept for ion propulsion.[6–8] A prototype variable specific impulse rocket (VASIMR) that uses hot plasma confined in an asymmetric magnetic mirror and exhausted through a magnetic nozzle to generate thrust is currently under investigation at the Johnson Space Center (JSC).[6,7] To generate their initial He or H_2 plasma, the JSC is using a helicon plasma source. It is obvious that for space operation, electron temperature measurements of the source must preferentially be simple, nonintrusive, and maintenance free.

Contrary to probes, spectroscopic measurements are not affected by rf fields, do not contaminate the plasma, and require little or no maintenance. A spectroscopic technique based on the relative intensities of neutral helium lines is used to measure the electron temperature in the HELIX (Hot hELIcon eXperiment)[9] plasma. This nonintrusive diagnostic relies on the fact that the electron impact excitation rate coefficients for helium singlet and triplet states differ as a function of the electron temperature. This method provides a line-of-sight averaged electron temperature of the plasma whereas a Langmuir probe gives a local measurement of the same plasma parameter. Since first proposed by Cunningham,[10] this line ratio diagnostic has been used to measure electron temperatures in many plasma conditions.[11–17] Recently, this technique has been considerably improved and extended to high-density, fusion edge plasmas.[18–23] Until now, the validity of this technique to

measure the electron temperature in rf generated plasmas has never been established.

At low densities ($n_e < 10^{11}\,\mathrm{cm}^{-3}$), the steady-state corona (SSC) model[24] can be used to determine the electron temperature with reasonable accuracy. This model assumes that the population of the emitting level is exclusively due to excitation from the ground state. Hence, helium electron impact excitation cross-sections from the ground state are taken from a database[25] and excitation rate coefficients calculated assuming a Maxwellian electron velocity distribution. The electron temperature is then obtained by measuring the intensity ratio of He transitions from the plasma.

At higher densities, secondary processes (excitation transfer, excitation from metastable) are no longer negligible, and the SSC model can no longer be used. Under these high-density conditions, collisional radiative (CR)[19,20] models must be used to predict the temperature. These complex models take into account many of the secondary processes and no longer assume that excitation is exclusively from the ground state. Apart from their inherent complexity, a major drawback of CR models is that many of the excitation transfer cross-sections are poorly known. In most CR models, theoretical expressions are used to evaluate missing excitation transfer cross-sections. The theoretical calculations and rare experimental values often differ by an order of magnitude or more.[26,27]

The wide range in density achievable in the HELIX plasma device (for He, $10^9 \leqslant n_e < 5\times10^{12}\,\mathrm{cm}^{-3}$, $5 \leqslant T_e \leqslant 20\,\mathrm{eV}$) enables us to verify to what extent this line ratio diagnostic can be used to predict the electron temperature in an rf plasma. After selecting suitable transitions, we measured line intensity ratios for a number of plasma conditions while simultaneously measuring both electron temperature and plasma density with a Langmuir probe. For 10 eV plasmas, line ratios obtained by spectroscopy are compared to the predicted values given by the different models available as a function of the plasma density. A discussion identifies the dominant secondary processes observed at higher density that invalidate the SSC model predictions.

II. EXPERIMENTAL APPARATUS

The WVU helicon source HELIX generates a steady-state plasma in a 1.60 m long cylindrical vacuum chamber with a 0.15 m diameter. The present chamber is composed of two distinct sections: a glass section (0.60 m long) where the copper antenna wraps around the tube and couples rf radiation into the plasma and a metal section with ports distributed along its length for diagnostics (see Fig. 1). This metal section is in turn attached at one end to a large aluminum space chamber (4.5 m long, 2 m inner diameter). Three turbomolecular drag pumps with a total pumping speed of 3700 l/s are connected to the vacuum chamber. The base pressure in the system is 1×10^{-7} Torr. Any gas or gas mixture can be injected through a feedback controlled piezoelectric valve mounted in a flange at the end of the small chamber. Operating gas pressures range from 0.5 to more than 100 mTorr. The steady-state HELIX magnetic field is generated with ten electromagnets that produce an axial magnetic field of 0–1300 G.[9] A function generator supplies the rf modulation to a steady-state rf amplifier. The amplifier can supply up to 2 kW of rf power to the plasma through a standard π matching circuit over the 0.3–30 MHz frequency range. The injected power is limited by the quality of the match. An assortment of antennae can be used for experiments in HELIX: Nagoya type III,[28] saddle coil,[29] and fractional helical antenna.[30] For the experiments described in this paper, pure He plasmas are produced with a fractional helical antenna at 11 MHz. Other operating conditions such as filling pressure, magnetic field strength, and rf power are adjusted to produce the required plasma parameters (see Sec. IV).

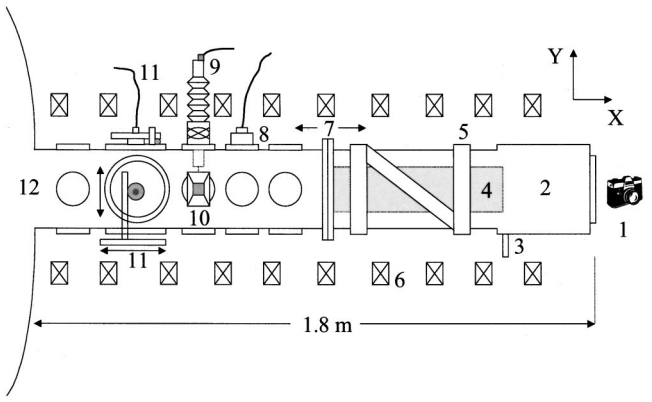

FIG. 1. Upper view of the HELIX plasma source. 1. Digital camera (near axial viewport), 2. Pumping station, 3. Gas inlet, 4. Plasma column, 5. Fractional helix antenna, 6. Magnetic field coils, 7. Glass chamber section (right), SS chamber section (left), 8. Spectroscopy optics, 9. Retractable rf compensated Langmuir probe, 10. Microwave interferometer, 11. 2D LIF injection and collection optics. 12. Large space chamber.

As shown in Fig. 1, the HELIX source is instrumented with an extensive array of diagnostics located in the metal section near the end of the antenna. These diagnostics include: a visible spectrometer system, a radially scanning rf compensated Langmuir probe, a microwave interferometer, and a laser induced fluorescence (LIF) diagnostic. The large space chamber is also instrumented with numerous diagnostics. These included a second radially scanning Langmuir probe, a radially scanning array of magnetic fluctuations sense coils, a radially scanning double probe for electrostatic fluctuation measurements, an LIF diagnostic, and a radially scanning differential energy analyzer.[31–35]

The spectrometer system is comprised of a Czerny-Turner 1.33 m scanning monochromator (wavelength range 185–1300 nm, holographic grating 1200 grooves/mm, *F*-number 11.6, dispersion 0.62 nm/mm, and with a maximum resolution of 0.015 nm) and, a charged coupled device (CCD) imaging camera (wavelength range 200–1100 nm, acquisition time from 10^{-2} s to several minutes, binning capability, 5.35 nm bandwidth, and a quantum efficiency between 0.2 and 0.55 over the sensitivity range). The CCD camera is operated under a dynamic background subtraction mode, which eliminates background noise from the signal. The light collection system used a 25 mm collimator lens mated to a silica fiber optics cable with matching numerical aperture. The light collection unit is located 0.35 m downstream from the end of the antenna. The detection area de-

fined by a light collection system at the center of the plasma chamber is 0.07 cm^2. A micro-positioning system is used to move the detection optics and a radial scan of the plasma column can be obtained. An absolutely calibrated light source is used to calibrate the response of the spectrometer at different wavelengths. Since we are using a line intensity ratio diagnostic, only a straightforward relative calibration is needed. For any HELIX plasma conditions, photon count fluctuations represent 1% of the total integrated intensity except at low plasma densities ($n_e < 3\times10^{10}\,cm^{-3}$) where they can reach up to 5%. The uncertainty related to re-absorption is less than 1% for most plasma conditions. Re-absorption uncertainty increases with plasma density and reach 1.1% at $n_e = 1\times10^{12}\,cm^{-3}$ for the 471.3 nm triplet transition (remains negligible for the 504.8 nm singlet transitions). The uncertainty associated with the relative calibration is about 2% for each wavelength.[36,37] Thus the resulting uncertainty on the line ratio measurements are about 8% at low plasma densities, and less than or equal to 3.4% for the rest of the density range covered in this paper.

The rf compensated Langmuir probe includes two modifications have been made to a standard Langmuir probe.[2,3] The first is the addition of a floating electrode. The electrode is exposed to the plasma potential fluctuations and is connected to the Langmuir probe tip via a capacitor. This helps to lower the sheath impedance and forces the Langmuir probe tip to follow the plasma potential oscillations, thereby reducing the distortion in the $I-V$ trace. The second modification is a chain of rf chokes. These are placed after the probe tip, but before the current is measured. The chokes increase the impedance of the circuit at the rf frequency. The Langmuir probe is connected to a high impedance source meter that sweeps the voltage and records the collection current. After a number of sweeps, the data are averaged and recorded by a computer. The probe is located 0.15 m downstream from the optical window (0.50 m from the antenna). The probe is mounted on a 0.15 m translator with an integrated position vernier. This arrangement enables both radial temperature and density profiles of half of the plasma column. The uncertainty relative to the position of the probe tip in the plasma column is ±1 mm. Observations (digital camera) of the plasma column from a large viewport located at the front end of HELIX (see Fig. 1) indicate that the plasma is symmetrical around the central *x*-axis. Line intensity measurements performed with and without the probe in the plasma (the probe is fully retractable) show no difference. A microwave interferometer is used to calibrate the Langmuir probe. The horns are located at exactly the same axial position as the Langmuir probe (the horns occupy the flanges located at 90° and 270° from the probe flange, see Fig. 1). The microwave interferometer uses direct measurements of phase shifts due to the plasma to determine the line-integrated electron density.[35] Electron temperatures are also measured with the second probe located in the large space chamber (1.5 m downstream from the first probe). Between the two probes, no significant difference in electron temperature is observed under most plasma conditions. Generally, the electron temperature in the large chamber is about 1 eV cooler than the temperature in HELIX.

Under steady-state plasma conditions, successive electron temperature measurements produce almost identical $I-V$ curves. Typically, electron temperature fluctuations are within 0.2 eV ($\approx$2%). The resulting uncertainty is more difficult to evaluate since the extraction of the electron temperature from the $I-V$ curve is based on an approximate theory.[2,38] Based on this fact and on previous experiments with Langmuir probes in helicon plasma,[9,31–35] we evaluate this uncertainty to about $\pm$15%. Plasma densities are evaluated by considering the ion saturation current section of the $I-V$ curve (modified Langmuir equation or Allen equation[38,39]). Again, repeatability in density values under steady-state plasma condition is excellent. Density fluctuations within 5% are observed under every plasma conditions. Including uncertainties from the area of the probe, the microwave calibration, the electron temperature, and the ion saturation, the resulting uncertainty for the plasma density is within $\pm$15%.

III. LINE RATIO DIAGNOSTIC

The link between measured line intensity ratio and plasma electron temperature is complex and a number of issues must be examined for the diagnostic. In particular, the different processes associated with the formation of excited levels populations responsible for the chosen atomic transitions must be well understood in order to extract information relative to the electron temperature of the plasma.

A. Line intensity from the plasma

The plasma emits radiation that is collected by the spectrometer through the fiber optics interface. The plasma emissivity ϵ_{ji} (W/vol·solid angle) at a specific wavelength λ_{ji} corresponding to an atomic transition from level *j* to level *i*, can be written as:[40]

$$\epsilon_{ji} = (4\pi)^{-1} h\nu_{ji} N_j A_{ji}, \tag{1}$$

where $h\nu_{ji}$ is the photon energy associated to the transition, N_j is the population of the emitting level (cm^{-3}), A_{ji} is the Einstein coefficient for the transition. Assuming a uniform plasma, the photon count rate I_p (λ_{ji}) measured by the CCD camera at wavelength λ_{ji} is given by:

$$I_p(\lambda_{ji}) = (4\pi)^{-1} N_j A_{ji} V \Omega T(\lambda_{ji})\,\eta(\lambda_{ji}), \tag{2}$$

where V is the plasma volume seen by the monochromator, Ω is the solid angle subtended by the collection optics, $T(\lambda_{ji})$ is the transmission factor of the detection system, and $\eta(\lambda_{ji})$ is the CCD camera quantum efficiency at wavelength λ_{ji}. Thus the ratio of the photonic count rate for two lines (wavelength λ_{ji} and λ_{kl}) is:

$$\frac{I_p(\lambda_{ji})}{I_p(\lambda_{kl})} = \frac{N_j A_{ji} T(\lambda_{ji})\,\eta(\lambda_{ji})}{N_k A_{kl} T(\lambda_{kl})\,\eta(\lambda_{kl})} = \frac{1}{F_R}\frac{N_j A_{ji}}{N_k A_{kl}}, \tag{3}$$

where the $T(\lambda)\ \eta(\lambda)$ products are associated with the response of the detection system at a given wavelength. Using an absolutely calibrated radiation source,[36,37] a calibration of the detection system at the two wavelengths is performed, yielding the relative calibration factor F_R.

B. Steady-state corona model

According to McWhirter,[24] the steady-state corona (SSC) model can be used to predict the population of excited levels provided the plasma condition satisfies the applicability criteria for the model. For this model the following conditions must be valid: the electron velocity distribution can be described by a Maxwellian; the ion and neutral temperatures are less than or equal to the electron temperature; the plasma is optically thin to its own radiation. The assumption that the electron velocity distribution is Maxwellian may not be absolutely accurate in helicon plasmas because of the controversial presence of hot electrons.[41–48] However, after extensive unsuccessful efforts to clearly detect the presence of these electrons, it is now generally accepted that the hot electron population is either very small compared to the thermal electron population or that no hot electrons are present during the steady-state operation of helicon devices.[47,48] We find no indication of hot electrons in either the Langmuir probe $I-V$ curve or in the spectroscopic data obtained in numerous emission experiments at low and high plasma densities. Furthermore, a spectroscopic experiment performed on Ar helicon plasmas[48] clearly indicates that excitation rate coefficients calculated for Maxwellian electron velocity distributions correctly describe the plasma radiation. Therefore, we will assume that hot electrons represent at best a negligible fraction of the entire distribution and that the distribution is essentially Maxwellian. It is consistent with this model that only a small fraction of the neutral or ion populations are in one of their possible excited states with respect to the ground state. In this model, a balance between the rate of collisional excitation from the ground state and the rate of spontaneous radiative decay determines the population densities of the excited levels.

As a first step, assume that all excitations are the result of single collisions between electrons and atoms in the ground state and that all applicable criteria for the SSC model are satisfied. Then, the population of the level $j(N_j)$ is given by the expression:[24]

$$n_e N_0 \langle \sigma v \rangle_{0j} = N_j \Sigma_{i<j} A_{ji}, \tag{4}$$

where N_0 is the population of the ground level population, n_e is the electron density, $\Sigma_{i<j}A_{ji}$ is the total transition probability from level j to all lower states, and $\langle \sigma v \rangle_{0j}$ is the excitation rate coefficient for the electron impact excitation of the level j from ground state. Cross-sections for electron impact excitation from He ground state to the different excited levels are used to evaluate the excitation rate coefficients. The cross-sections have been measured by a number of researchers (crossed-beam experiments) and compilations are available.[25,49–52] The excitation rates used in this paper are taken from the Kato and Janev compilation.[50] The line ratio expressed in terms of excitation rate coefficients becomes:

$$R_1(T_e) = \frac{I_p(\lambda_{ji})}{I_p(\lambda_{kl})} = \frac{1}{F_R}\frac{\langle \sigma v \rangle_{0j} B_{ji}}{\langle \sigma v \rangle_{0k} B_{kl}} = \frac{1}{F_R}\frac{E_{ji}(T_e)}{E_{kl}(T_e)}, \tag{5}$$

where $B_{ji} = A_{ji}(\Sigma_{i<j}A_{ji})^{-1}$ is the "branching ratio" (transition probability for a specific transition from level j on the total transition probability from level j), and $E_{ji}(T_e)$ is the emission rate coefficient $[E_{ji}(T_e) = B_{ji}\langle \sigma v \rangle_{0j}]$. In this model, the line intensity ratio function $R_1(T_e)$ depends solely on the electron temperature in the plasma. The SSC model is believed to be able to predict the electron temperature with reasonable accuracy for electron densities up to $10^{11}\,\mathrm{cm}^{-3}$. At higher densities, secondary processes (excitation transfer between neighboring levels, excitation from metastable levels) are increasingly important and a different model is needed to predict the electron temperature.

C. Secondary processes, metastable contributions

The SSC model assumed that line emission is the result of single collisions between electrons and atoms in the ground state followed by direct radiative de-excitation. At higher densities, this assumption is no longer valid since the occurrence of secondary processes involving collisions with excited or ionized atoms becomes important. The secondary processes include: volume recombination (recombination collisions contribute to the emitting level population); collisions between excited atoms and ground state atoms (by this mechanism a highly excited atom can lose part of its excitation to another atom in the ground state resulting in one or two more excited atoms); cascading redistribution effects [this process involves the electron impact excitation of a highly excited level followed by transition(s) to the upper line levels]; excitation transfer collisions (the upper line levels can be populated or depopulated by excitation transfer collisions); excitation from metastables (the upper line levels can be excited through collisions between electrons and the metastable states of the atom).

We limit this discussion to low temperature, low to moderate density He plasmas ($T_e \leqslant 20\,\mathrm{eV}$, $n_e \leqslant 1\times10^{13}\,\mathrm{cm}^{-3}$) where several of these secondary processes can be neglected. The effect of volume recombination is negligible since the recombination rate at these filling pressures is much smaller than the excitation rate.[17] The effect of collisions between excited and ground atoms is negligible since the ion neutral collision time is much longer than the upper line de-excitation period. The cascading redistribution effect will be important if the electron temperature is comparable to the upper line level energy. Since the first excited level of the He atom is at 19.81 eV,[51] redistribution effects for higher levels ($n>2$) can be neglected. The excitation transfer collisions effect will be important if the upper line level has neighboring level(s) with about the same energy. Excitation transfer cross-sections are also larger when transitions between levels are optically allowed.[26] Finally, excitation contributions from the metastable levels can be important if the metastables are close to the ground state (large metastable population) or if metastables are energetically close to the emitting excited levels.

Fortunately, contributions from the metastable levels can be accurately evaluated using a collisional radiative (CR) model. The model makes predictions for the metastable populations and known excitation cross-sections from the metastable levels[26,27] are used to modify the line intensity ratio calculation. These contributions can be integrated in the

line ratio expression by replacing the emission rate coefficients by an apparent or resulting emission rate coefficient $E^*_{ji}(T_e,n_e)$ and $E^*_{kl}(T_e,n_e)$ that include both direct (ground) and indirect (metastables) excitation:

$$R_1(T_e,n_e)=\frac{1}{F_R}\frac{E^*_{ji}(T_e,n_e)}{E^*_{kl}(T_e,n_e)}. \tag{6}$$

This line intensity ratio function is essentially the SSC model corrected for metastable contributions. The line ratio becomes a function of both electron temperature and plasma density. Excitation transfer contributions cannot easily be incorporated into the SSC model. However, since they are the only non-negligible secondary process unaccounted for, a comparison between the modified SSC model and experimental data can reveal the importance of excitation transfer contributions to the resulting line ratio.

D. Collisional radiative model

A collisional radiative (CR) model can also be used to predict the electron temperature. The essential difference between the corona model and the CR model is that the latter model no longer assumes that bound excited populations originate exclusively from the ground state via electron impact excitation. In this model, secondary processes like excitation transfer, recombination, and ionization involving all excited states are included in the computation. In order to use this model, the plasma must satisfied the following conditions:[24] the electron velocity distribution can be described by a Maxwellian; the ionization process is by electron collision from any bound level and is partially balanced by three-body recombination into any level; excitation transfer between any pair of bound level are induced by electron collisions; radiation is emitted when a bound electron makes a spontaneous transition to a lower level or when a free electron makes a collisionless transition into a bound level; the plasma is optically thin especially to its own resonance radiation. With these assumptions a set of equations describing the population of bound levels N_i can be written as:[20]

$$dN_i/dt=n_e\Sigma_{j\neq i}S_{ji}N_j+\Sigma_{j>i}A_{ji}N_j-n_e\Sigma_{j\neq i}S_{ij}N_i -\Sigma_{j<i}A_{ij}N_i-n_eI_iN_i=0. \tag{7}$$

The S_{ij} (excitation or de-excitation rate coefficients) and I_i (ionization rate coefficients) are all functions of electron temperature and plasma density. The first term corresponds to the excitation or de-excitation of the electron population of all levels *j* that end up at level *i*. The second term corresponds to the spontaneous de-excitation (allowed transitions) from higher *j* levels to level *i*. The third term is associated with the excitation or de-excitation of level *i*. The fourth term is the spontaneous de-excitation (allowed transitions) originating from level *i*. The last term is associated with the ionization rate of the electron population of level *i*. Each level of the He atom is described by a similar equation. A system of *N* (level number) coupled differential equations must be solved simultaneously to obtain the population of a given level. The operation is repeated for the second transition and Eq. (4) can then be used to determine the electron temperature from the line intensity measurement. For the He atom, the second and fourth terms on the right side of Eq. (7) can be evaluated accurately since the A_{ij} coefficients are well known.[53,54] However, the picture is quite different for the remaining terms. The excitation (or de-excitation) cross-sections of short-lived excited state are poorly known. Theoretical calculations[26] are often used to fill the missing rate coefficients. Cross-sections obtained by different models can differ by one or more orders of magnitude at low electron energy.[26,27]

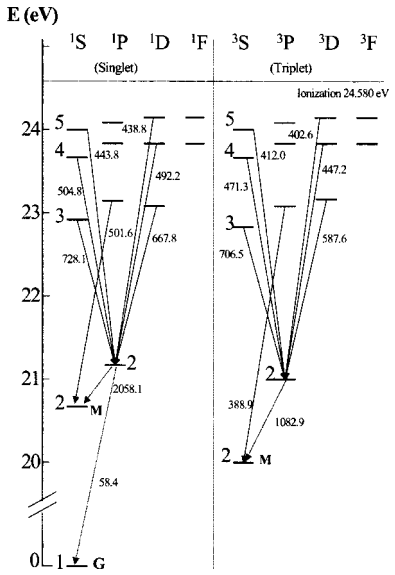

FIG. 2. Partial Grotrian diagram of the helium atom with some important transitions (λ in nm). Visible transitions (full line), infra red, and ultraviolet lines (hash line). G and M are for ground and metastables states, respectively.

E. Helium transitions

To measure the plasma electron temperature from a line ratio, a careful selection of emission lines must be made. First, the line ratio of the selected transitions must depend as much as possible on the electron temperature and as little as possible on the electron density. Since secondary effects are strongly density dependent, we must select transitions for which secondary effects have limited importance on the resulting intensities. The radiation must also escape from the plasma without being re-absorbed (the plasma must be optically thin). Finally, these transitions must be in the detection and sensitivity range of the spectrometer.

The He Grotrian diagram is shown in Fig. 2. The left side of the diagram features the singlet states while the triplet states are shown in the right side. The He atom has 2 metastables, namely the $2\,^1S$ state (singlet) and the $2\,^3S$ (triplet). The energy levels of the He atom are given in Table I. As seen in the Grotrian diagram, there are a number of possible transitions that can be used. Transitions originating from a level with principal quantum number $n>5$ will not be considered since the electron population of these higher levels becomes increasingly smaller with increasing *n*, resulting in weak transitions. Transitions ending at the ground state $1\,^1S$ and at metastable levels $2\,^1S$ and $2\,^3S$ will not be considered

TABLE I. Helium energy levels. Singlet (left) and triplet (right) states.

Level	Energy (eV)	Level	Energy (eV)
$2\,^1S$	20.610	$2\,^3S$	19.814
$2\,^1P$	21.212	$2\,^3P$	20.958
$3\,^1S$	22.914	$3\,^3S$	22.712
$3\,^1P$	23.081	$3\,^3P$	23.001
$3\,^1D$	23.068	$3\,^3D$	23.067
$4\,^1S$	23.667	$4\,^3S$	23.588
$4\,^1P$	23.736	$4\,^3P$	23.730
$4\,^1D$	23.730	$4\,^3D$	23.730
$4\,^1F$	23.731	$4\,^3F$	23.731
$5\,^1S$	24.005	$5\,^3S$	23.965
$5\,^1P$	24.039	$5\,^3P$	24.022
$5\,^1D$	24.036	$5\,^3D$	24.036
$5\,^1F$	24.037	$5\,^3F$	24.037

since the plasma is not optically thin with respect to these transitions and the resulting intensities are strongly affected by re-absorption. There are two reasons to avoid $D\rightarrow P$ transitions. First, excitation transfer cross-sections for allowed transitions are much larger than for nonallowed transitions.[26] Second, the excitation transfer is inversely proportional to the energy difference between levels and strongly dependent on plasma density. For example, the energy difference between the $3\,^1P$ and $3\,^1D$ levels is only 0.013 eV while the corresponding quantity between the $3\,^3P$ and $3\,^3D$ levels 0.066 eV. For the $n=4$ level, $\Delta E(4\,^1P/4\,^1D)$ is only 0.006 eV while $\Delta E(4\,^3P/4\,^3D)$ is even smaller. Thus these transitions will be more sensitive to plasma density than electron temperature.[19]

Line ratios using $S\rightarrow P$ transitions are better suited to measure electron temperature. The contributions from the metastable $2\,^1S$ and $2\,^3S$ states due to excitation transfer are small since these S-S transitions are forbidden and the resulting cross-section are small.[26] Also, for a given n level, the energy of the S levels is significantly different than the energy of the other P, D, or F levels. Thus excitation transfer cross-sections between S and any of these P, D, or F levels are also small compared to cross-sections involving only P, D, and F levels.

The possible transitions for the diagnostic together with their respective transition probability and branching ratio are listed in Table II. The $3\,^1S\rightarrow 2\,^1P\,(728.1\,\text{nm})/3^3\rightarrow 2\,^3P\,(706.5\,\text{nm})$ ratio is attractive for a number of reasons. First, both transitions are within the same spectral region. Second, these transitions are very intense since both originate from the $n=3$ level. Third, they have exactly the same branching ratio (see Table II). Finally, a CR model has been used previously to predict electron temperature from this line ratio as a function of plasma density.[19] The only potential problem associated with these transitions is the close proximity of the metastable levels. The excitation contributions from the metastable levels will be the largest among the possible transition pairs.[17] This close proximity will also result in significant plasma re-absorption of the emission lines (see the next section).

TABLE II. Singlet and triplet transitions, transition probabilities, and branching ratios.

Transition	λ (nm)	$A_{ji}(\times 10^8\,\text{s}^{-1})$	B_{ji}
$5\,^1S\rightarrow 2\,^1P$	443.8	0.0330	0.482
$4\,^1S\rightarrow 2\,^1P$	504.8	0.0675	0.596
$3\,^1S\rightarrow 2\,^1P$	728.1	0.1829	1.000
$5\,^3S\rightarrow 2\,^3P$	412.0	0.0444	0.475
$4\,^3S\rightarrow 2\,^3P$	471.3	0.0955	0.596
$3\,^3S\rightarrow 2\,^3P$	706.5	0.2790	1.000

The $4\,^1S\rightarrow 2\,^1P\,(504.8\,\text{nm})/4\,^3S\rightarrow 2\,^3P\,(471.3\,\text{nm})$ ratio is equally attractive. These transitions are in the same spectral region and have similar branching ratios. Their intensities are weaker than the preceding pair but still easily detectable. Being energetically further apart from the metastables than the $n=3$ transitions, they are less affected by excitation transfer from these levels. Two different CR models have been used to determine electron temperature from this line ratio as a function of plasma density.[19,20]

The $5\,^1S\rightarrow 2\,^1P\,(443.8\,\text{nm})/5\,^3S\rightarrow 2\,^3P\,(412.0\,\text{nm})$ ratio is also a valid selection. Again, these transitions are in the same spectral region and have similar branching ratios. Originating from the $n=5$ level they are minimally affected by the metastable levels. The main drawback for these transitions is their relative weakness when compared to the other pairs. The small difference in energy between all the $n=5$ levels is also conducive to large excitation transfer rates between levels. No CR model has been used to predict temperature from this line ratio. Although it may be possible and potentially advantageous (the line ratio would increase/decrease rapidly as a function of T_e) to compare two lines originating from different principal quantum levels, the large difference in intensity (>10) and, the important difference in wavelength makes such an approach more prone to imprecision.

F. Optical escape factor and mean optical depth

Line intensities associated with transitions of plasma species (neutral or ion) are the result of spontaneous emission, stimulated emission, and absorption. In order to use line intensity for any diagnostic, one must first examine if the plasma optically affects a specific transition. A line is optically thin if both stimulated emission and absorption are negligible compare to spontaneous emission. In this case, the line intensity $I(\nu)$ of that transition is given by Eq. (1). The plasma is optically thick (or opaque), if the absorption process is dominant and only a small fraction of the emitted light escapes the plasma. Plasmas are generally optically thin when electron densities are low ($<10^{10}\,\text{cm}^{-3}$) but are increasingly opaque as density increases. In general, the plasma is opaque to resonance lines (transitions involving the ground state) and for transitions ending on metastable levels, but remains optically thin for transitions between excited levels even at moderately high density ($\geqslant 10^{14}\,\text{cm}^{-3}$). However, in certain cases, the proximity of a metastable level can affect the opacity of the plasma for a given transition. The two important parameters to quantify the opacity of the plasma are the optical escape factor (OEF) and the mean optical depth (MOD). The OEF corresponds to the fraction

TABLE III. Mean optical depth (τ_0) and optical escape factor (Λ) for six He transitions at different plasma densities (10^{11}, 10^{12}, 10^{13}, and $10^{14}\,\mathrm{cm}^{-3}$).

λ (nm)	τ_0	Λ	τ_0	Λ	τ_0	Λ	τ_0	Λ
	($n_e=10^{11}\,\mathrm{cm}^{-3}$)		($n_e=10^{12}\,\mathrm{cm}^{-3}$)		($n_e=10^{13}\,\mathrm{cm}^{-3}$)		($n_e=10^{14}\,\mathrm{cm}^{-3}$)	
412.0	1.85 e-3	0.9987	1.45 e-2	0.9898	3.00 e-2	0.9790	2.25 e-2	0.9841
443.8	1.79 e-6	1.0000	1.72 e-5	1.0000	1.72 e-4	0.9999	1.50 e-3	0.9989
471.3	2.00 e-3	0.9986	1.55 e-2	0.9890	3.20 e-2	0.9777	2.45 e-2	0.9825
504.8	1.90 e-6	1.0000	1.80 e-5	1.0000	1.80 e-4	0.9999	1.60 e-3	0.9989
706.5	6.65 e-2	0.9542	4.61 e-1	0.7285	8.45 e-1	0.5666	7.15 e-1	0.6158
728.1	4.55 e-5	1.0000	4.40 e-4	0.9997	4.40 e-3	0.9969	3.85 e-2	0.9733

of light that can escape the plasma; for OEF equal or close to unity, the plasma is optically thin. The MOD is the exponential absorption coefficient associated with a given transition ($I=I_0e^{-\tau_0}$). An MOD smaller than or equal to 0.01 corresponds to an optically thin plasma.

To evaluate the MOD and OEF values for each transition we used the differential radiative transfer equation that includes both emission and absorption processes in the plasma.[55,56] Assuming that for He transitions the dominant broadening mechanism is Doppler broadening,[57] the mean optical depth τ_0 and the optical escape factor $\Lambda(\tau_0)$ are given by the following expressions:[24,58,59]

$$\tau_0=\tau(\nu_0)=\frac{n_1 g_2 A_{21}\lambda_0^3 r}{8g_1\pi^{3/2}\nu_{\mathrm{th}}}, \tag{8}$$

$$\Lambda(\tau_0)=1-\left(\frac{\tau_0}{\sqrt{2}}-\frac{\tau_0^2}{\sqrt{3}2!}+\frac{\tau_0^3}{\sqrt{4}3!}\ldots\frac{(-1)^{n+1}\tau_0^n}{\sqrt{n+1}n!}\right), \tag{9}$$

where n_1 is the population of the lower level, g_1 and g_2 are, respectively, the statistical weight of the lower and upper levels, A_{21} and λ_0 are the transition probability and central wavelength value associated with the transition, v_{th} is the thermal velocity of He, and r is a characteristic length of the plasma (radius).

According to Eq. (8) the mean optical depth depends on the lower excited level, not on the population of the upper level. In order to evaluate the lower excited populations ($2\,^1P$ and $2\,^3P$), we must first evaluate the neutral population in the plasma column. We consider a plasma with a filling pressure of 10 mTorr and with a 1.5 cm radius column. At this pressure, the electron temperature is about 10 eV and the average neutral temperature measured by LIF is about 0.05 eV (580 K).[4] Thus the neutral density in the plasma column is about $1.7\times10^{14}\,\mathrm{cm}^{-3}$. For an electron temperature of 10 eV, the populations of the $2\,^1P$ excited level are, according to Broda's collisional radiative model,[19] equal to 0.007, 0.068, 0.680, and, $5.95\times10^{9}\,\mathrm{cm}^{-3}$ for plasma densities of 10^{11}, 10^{12}, 10^{13}, and $10^{14}\,\mathrm{cm}^{-3}$, respectively. Similarly, the $2\,^3P$ level populations predicted by the model are 0.06, 0.51, 1.1, and, $0.79\times10^{11}\,\mathrm{cm}^{-3}$ for the same density values, respectively. Comparable population values are also obtained with Sasaki's model.[20] Note that the $2\,^3P$ populations are typically 100 times larger than the corresponding $2\,^1P$ populations. Note also that the $2\,^3P$ population at $n_e=10^{13}\,\mathrm{cm}^{-3}$ is larger than the corresponding population at $10^{14}\,\mathrm{cm}^{-3}$. Here, the electron-impact depletion of the $2\,^3S$ metastable level (and by consequence of the $2\,^3P$ level) is responsible for this situation.[19,20] The statistical weights g_1 and g_2, the wavelengths and the transition probabilities A_{ji} are available in the literature.[53] Using Eqs. (8) and (9), the MOD and OEF for the He transitions discussed previously are shown in Table III as a function of plasma density.

For all singlet transitions, the OEF is essentially unity and the plasma is optically thin, even for electron densities up to $10^{14}\,\mathrm{cm}^{-3}$. For the triplet transitions, the situation is somewhat less favorable. Essentially, transitions from the upper levels $5\,^3S$ and $4\,^3S$ (412.0 and 471.3 nm, respectively) can be considered as optically thin for plasmas with electron densities up to $10^{14}\,\mathrm{cm}^{-3}$ (less than 2% of re-absorption in each case). Meanwhile, the transition from the $3\,^3S$ level (706.5 nm) is largely re-absorbed by the plasma ($\approx$5% at $10^{11}\,\mathrm{cm}^{-3}$, $\approx$43% at $10^{13}\,\mathrm{cm}^{-3}$, and, $\approx$40% at $10^{14}\,\mathrm{cm}^{-3}$). A combination of factors is responsible for this situation. Specifically, a strong transition (large A_{ji}), a large n_1 population (due to the presence of the long-lived $2\,^3S$ metastable near the $2\,^3P$ level) and a long wavelength ($\tau_0\propto\lambda_0^3$) all contribute to make the MOD large enough so that the plasma is no longer transparent to this transition. Thus the 706.5 nm line intensity must be corrected for re-absorption. Since re-absorption is a function of the neutral density profile and of the dominant broadening mechanism, the correction is nontrivial. If possible, the line ratio diagnostic should not use this transition.

Different HELIX plasma conditions will yield comparable MOD and OEF values since the different T_e, n_1, and v_{th} values act as check-and-balance factors in Eq. (8). It is important to observe that it is the combination of large excited population ($2\,^3P$ level) and high plasma density that is responsible for re-absorption. This suggests that the correction for re-absorption can be small if the He gas is injected in H_2 plasma (or other gases). Thus the 706.5 nm line can be used as part as a line ratio diagnostics in high density Tokamak plasmas as long as the local density of the He [and thus He($2\,^3$P)] population remains small.[21–23]

IV. EXPERIMENTAL RESULTS

The rf compensated Langmuir probe was used to radially scan the plasma column. By nature, the probe provides *in situ* temperature and density measurements while the spectroscopy-derived values are line-of-sight averaged measurements. Since the line intensity is proportional to the

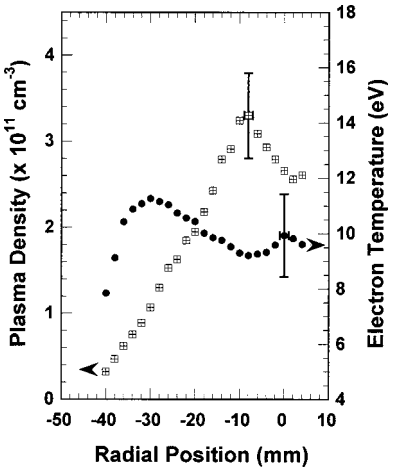

FIG. 3. Plasma density (circle) and electron temperature (square) as a function of the radial position in the plasma column. Discharge conditions: $|B|=1$ KG, Pressure=6.5 mTorr, Power=400 Watts.

number of emitters, the density profile of the species responsible for emission (neutral and electron) can play an important role in the resulting line ratio values. The neutral He profile is assumed to be uniform in the plasma since the ionization fraction of the plasma remains small (less than 1% in all cases). Typical plasma density and electron temperature profiles are shown in Fig. 3. The plasma is assumed to be symmetric around the central axial position identified as the zero position. The symmetric nature of the plasma column is confirmed by observation of the plasma with a digital camera[60] from the viewport located at the front end of HELIX (see Fig. 1). Typically, the He plasma column produced in HELIX can be described in terms of a ''fill'' ring shape with maximum density located at about 1 cm from the central axis position. The maximum density position is a function of the magnetic field strength. Similar plasma configurations have been observed elsewhere[30,61–64] and are associated with the presence of the $m=+1$ helicon mode in the plasma. Little change in the density profile has been observed for magnetic field strengths ranging from 300 to 1200 G. The maximum density shifts toward the tube center and the plasma becomes less hollow as B increases. To minimize this effect and to ensure that most of the radiation comes from the central plasma ''core,'' all of the line ratio measurements were performed with magnetic field strength from 600 to 1200 G.

As shown in Fig. 3, the maximum electron temperature is often observed away from the center of the discharge. However, the average electron temperature in the bulk of the plasma column does not significantly differ from the average electron temperature in the plasma core. All measured electron temperature profiles show the same behavior. Spatially periodic electron temperature oscillations in the profile are frequently observed and are presently not understood. For almost all plasma conditions, these oscillations remained small (± 1 eV) as seen in Fig. 3. Only near transitions between helicon modes are large amplitude oscillations observed. Such often-unstable plasma conditions were not used for the experiments reported here.

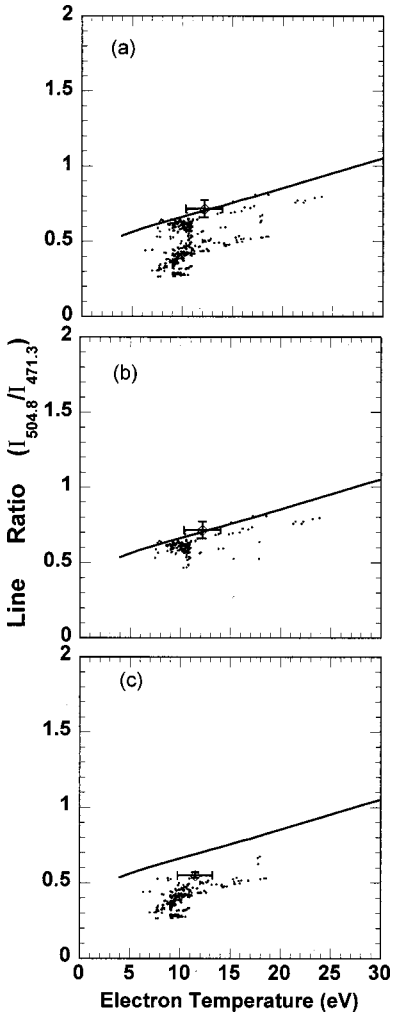

FIG. 4. (a) Line ratio versus electron temperature as measured by the Langmuir probe. Data points: measured line ratio; solid line SSC model prediction. Almost all of the experimental points are below the SSC model line function. (b) Line ratio versus electron temperature for plasma density below $10^{11}\,\mathrm{cm}^{-3}$. The points are within a few percent of the SSC model line function. (c) Line ratio versus electron temperature for plasma density above $10^{11}\,\mathrm{cm}^{-3}$. The experimental points are systematically below the SSC model line function.

Since most of the line emission comes from the central core, the Langmuir probe tip was placed in the plasma ring where the plasma density was maximum. More than 400 line ratios were measured under a wide range of plasma conditions. All probe measured electron temperatures as well as temperatures calculated from the SSC model are shown in Fig. 4(a). In Fig. 4(b), line ratio based temperature values for plasma densities lower than $10^{11}\,\mathrm{cm}^{-3}$ are shown. Line ratio temperature values for plasma densities higher than $10^{11}\,\mathrm{cm}^{-3}$ are shown in Fig. 4(c). The data clearly indicate that for $n_e<10^{11}\,\mathrm{cm}^{-3}$ the SSC model can be used to determine the electron temperature with reasonable accuracy. For $n_e>10^{11}\,\mathrm{cm}^{-3}$, the line ratio always underestimates the plasma temperature and the SSC model can no longer be used. At these densities, the emission from the triplet state increases faster as a function of plasma density than the radiation coming from the singlet state.

The line intensity for the two transitions as a function of

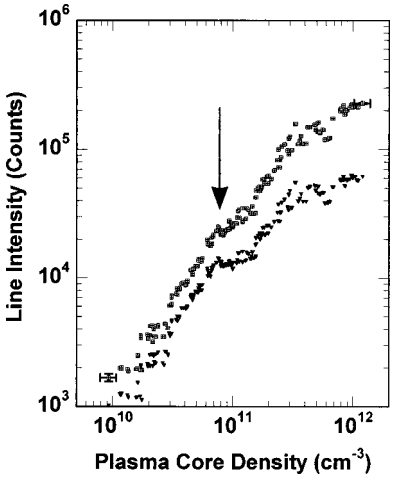

FIG. 5. Triplet (square) and singlet (triangle) integrated line intensities as a function of plasma density. The slope of the two signals remains the same up to a density of $8\times10^{10}\,\mathrm{cm}^{-3}$ (arrow), then the two slopes diverge.

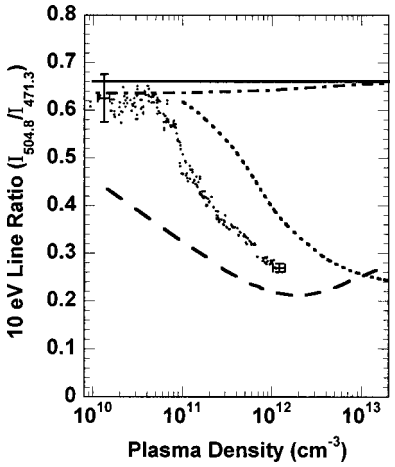

FIG. 6. 10 eV Line ratio (504.8/471.3) as a function of plasma density. Experimental line ratios (solid circle), SSC model (solid line), SSC model +metastable contributions (alternative dot-dash line), corrected Sasaki CR model (large dash line), and Brosda CR model (dotted line).

the plasma density and for a given electron temperature (10 ± 1 eV) are shown in Fig. 5. The slopes of the two signals are the same up to a density of about $8\times10^{10}\,\mathrm{cm}^{-3}$. Above this density, the triplet radiation increases at a more rapid pace than its singlet counterpart. Two other features of Fig. 5 deserve comment. First, the highly correlated nature of the line emission indicates that electron impact excitation from the ground state remains an important component of the total excitation process of the emitting level even under high-density conditions. Also, local or temporal fluctuations in both n_e and T_e affect each line's emission in similar fashion. Second, that the line emission from the triplet state scales as the plasma density measured by the probe in the core (peak density). This confirms that most of the plasma radiation comes from the inner core.

To understand how plasma density specifically affects the line ratio, the line ratios are plotted as a function of plasma density in Fig. 6. Line ratio measurements for plasma densities ranging between 9.3×10^{9} and $1.24\times10^{12}\,\mathrm{cm}^{-3}$ and where the electron temperature in the core is within 10 ± 1 eV are shown in Fig. 6. Higher plasma densities are possible in the HELIX device, but only at lower electron temperature. The line ratio value predicted by the density independent SSC model at $T_e=10\pm1$ eV ($R=0.66\pm0.02$) is shown in Fig. 6. There is good agreement between the measured line ratios and the value predicted by the SSC model at low density ($n_e<8\times10^{10}\,\mathrm{cm}^{-3}$). This agreement validates the calibration and the selection of the atomic data (cross-sections and transition probabilities) used for this model. The agreement supports the conclusion that a negligible population of hot electrons is present in the plasma, as hot electrons would dramatically increase the line ratio value.

It has been suggested that the deviation from the corona model is primarily due to the metastable contributions.[13,14] Using Eq. (6) and assuming that the population of the $2\,^3S$ and $2\,^1S$ metastable states remains small when compared to the ground population, the line ratio function including metastable contributions can be written as

$$R_1(T_e,n_e)\approx\frac{[\langle\sigma v\rangle_{0\to4\,^1S}+f_{2\,^3S}\langle\sigma v\rangle_{2\,^3S\to4\,^1S}+f_{2\,^1S}\langle\sigma v\rangle_{2\,^1S\to4\,^1S}]B_{504.8}}{[\langle\sigma v\rangle_{0\to4\,^3S}+f_{2\,^3S}\langle\sigma v\rangle_{2\,^3S\to4\,^3S}+f_{2\,^1S}\langle\sigma v\rangle_{2\,^1S\to4\,^3S}]B_{471.3}},\tag{10}$$

where $f_{2\,^3S}$ and $f_{2\,^1S}$ are the relative populations (normalized by the ground state population N_0) of the $2\,^3S$ and $2\,^1S$ levels, respectively. The numerator terms correspond to the three different excitation processes that will populate the singlet upper level $4\,^1S$. The contributions are from the ground state, the $2\,^3S$ metastable, and the $2\,^1S$ metastable, respectively. The denominator terms are for the equivalent contributions to the $4\,^3S$ state. $B_{504.8}$ and $B_{471.3}$ are the branching ratios for the observed transitions. The metastable populations are a function of the plasma density and are taken from the Sasaki CR model[20] (similar population values are found with Brosda model). The $2\,^3S$ population slowly decreases as function of plasma density (from $0.002\ N_0$ at $n_e=10^{10}\,\mathrm{cm}^{-3}$ to $0.0008\ N_0$ at $10^{13}\,\mathrm{cm}^{-3}$) while the $2\,^1S$ slowly increases in the same range from 8×10^{-6} to $9\times10^{-6}\ N_0$. As result, the line ratio function increase from 0.636 to 0.655 through the 10^{10} to $10^{11}\,\mathrm{cm}^{-3}$ density range. The line ratio function is shown in Fig. 6. Up to a density of about $10^{11}\,\mathrm{cm}^{-3}$, the line ratio function predicted by this modified SSC model is in excellent agreement (within 2.5%) with the experimentally results. However, the model and the experimental data diverge significantly for higher densities.

Thus at higher plasma densities, metastable contributions are no longer the dominant secondary process. It is very likely that excitation transfer processes become the most important of the secondary processes for electron densities above $10^{11}\,\mathrm{cm}^{-3}$.

The line ratio values obtained by using two different collisional radiative (CR) models (Brosda and Sasaki) at $T_e = 10\,\mathrm{eV}$ are also plotted in Fig. 6. The Brosda CR model calculation, under the low-density limit ($n_e \rightarrow 1\,\mathrm{cm}^{-3}$), coincides with the SSC ratio value at 10 eV. This means that the atomic data values used by Brosda in his model are similar to the values used for our SSC model calculation. The general agreement between the Brosda CR model and the experimental data is good. The best agreement is observed at plasma densities up to $1.5\times10^{11}\,\mathrm{cm}^{-3}$. At higher density, the model predicts a higher line ratio value than what is observed experimentally. Note that the general trend for the line ratio function predicted by the model is also observed experimentally. One may argue that the difference between experiment and model might be due to the different plasma density values used by the code in comparison with the experiment. The model assumes a uniform density throughout the plasma column, while we used the peak plasma density. In fact, using the averaged measured density would move the experimental data away from Brosda curve and toward the Sasaki line ratio function.

The line ratio function predicted by the Sasaki CR model has been normalized by a factor of 1.2 and is also shown in Fig. 6. This correction was deemed necessary since the predicted line ratio value under the low-density limit ($n_e \rightarrow 1\,\mathrm{cm}^{-3}$) was 20% smaller than both the SSC value and Brosda CR model prediction. Careful examination of atomic data used by Sasaki *et al.*[20] revealed that their $1\,^1S \rightarrow 4\,^1S$ cross-section was underestimated by 20%. The line ratio function predicted by the Sasaki model is significantly different than the corresponding Brosda curve. By far, the most striking difference is that their predicted line ratios at low density ($\leqslant 10^{11}\,\mathrm{cm}^{-3}$) are significantly smaller than both the measured and calculated (Brosda) line ratios. This predicted behavior is incompatible with SSC model at low plasma densities. Since their predicted metastable populations are comparable to those calculated by Brosda,[19] this means that excitation transfer cross-sections used for their computation are much larger than those used by Brosda (the only other important mechanism that would reduce the line ratio as a function of plasma density).

At higher densities, agreement with the experiment improves. Note that the two models predict the same line ratio values for plasma densities of about $1\times10^{13}\,\mathrm{cm}^{-3}$. At plasma densities close to this latter value, the population of the different higher levels will tend to reflect their statistical weights plus the contribution associated with cascading effects from the upper levels.[20] The different configuration of the de-excitation scheme on each side of the Grotrian diagram will also favor the triplet emissions. On the singlet side, most of the excited electrons undergo de-excitation to the ground state (even the $2\,^1S$ metastable level has a small population with respect to the ground state). However, on the triplet side, a large portion of the upper levels de-excite toward the $2\,^3S$ metastable level since de-excitation toward the ground state (singlet) is highly forbidden.[65,66] Electrons from the $2\,^3S$ level are then quickly and predominantly re-excited in upper triplet states since the cross-sections for the triplet–triplet excitations are larger than the corresponding triplet-singlet cross-sections.[26] As result, emission from the populations of the triplet levels will always be much larger than the corresponding radiation from singlet levels. This is confirmed by estimated population numbers for the different levels using CR models.[19,20]

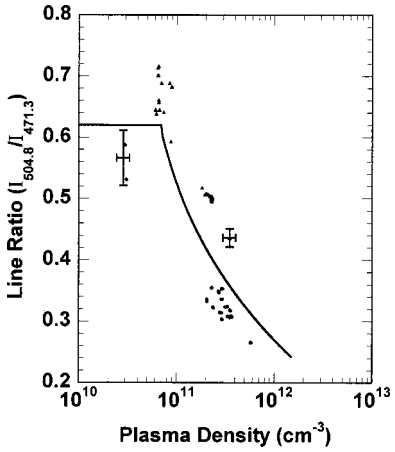

FIG. 7. Line ratio as a function of plasma density. Fit (solid line) for the 10 eV line ratio function as obtained from the experimental data (see Sec. IV). 7 eV line ratio values (solid circle), 12 eV line ratio values (solid triangle).

Of course, a fraction of these $2\,^3S$ metastables may be ionized instead of excited. The increasing importance of the ionization process as density increase may also explain why both models predict that the line ratio function in the 10^{12}–10^{13} range is becoming almost independent of density. This in turn strongly suggests that the path to ionization in He plasma is primarily through triplet states. Ultimately, with increasing density ($n_e > 10^{13}\,\mathrm{cm}^{-3}$), the ionization process becomes so important that it reduce triplet emission (depletion of the $2\,^3S$ population) and the line ratio function start to increase as a function of density. The two CR models have predicted this kind of behavior for their respective line ratio functions at high plasma densities.

A fit describing the experimental values line ratio function at $T_e = 10\,\mathrm{eV}$ is shown in Fig. 7. The fit is giving by:

$$R(n_e) = 0.62 \qquad n_e \leqslant 7\times10^{10}\ \ \mathrm{cm}^{-3}$$
$$R(n_e) = 461.5\,n_e^{-0.26916} - 1.9\ \ E9/n_e + 3.9\ \ E20/n_e^2 \qquad 7\times10^{10} < n_e < 1.3\times10^{12}\ \ \mathrm{cm}^{-3}.$$

A series of line ratio measurements performed at two other electron temperatures 7 ± 1 and 12 ± 1 eV are also shown in Fig. 7. As anticipated, the 12 eV line ratio values are systematically higher than the corresponding 10 eV values, while the 7 eV values are systematically lower. Although the data sampling for these two latter temperatures is much more limited than in the 10 eV case, the same general behavior of the line ratio as a function of plasma density is observed. Thus the fit to line ratio data are scalable for different electron temperatures within the plasma density range studied in this paper. This suggests that the 10 eV line ratio function could be extended beyond the $1.3\times10^{12}\,\mathrm{cm}^{-3}$ density limit by measuring the line ratio function of a lower temperature plasma and then scaling the result for the difference in electron temperature.

V. CONCLUSION

We have shown that a line ratio diagnostic can be used to determine the electron temperature in a helicon plasma source. For plasma densities lower than $8\times10^{10}\,\mathrm{cm}^{-3}$, the simple steady-state corona model can be used with reasonable accuracy. Addition of metastable contributions to the SSC model improves the agreement between theory and experiment. This result is incompatible with the presence of a large fraction of hot electrons in the helicon source electron distribution, even at low plasma density. For higher plasma densities a more complex collisional radiative model is needed. To our knowledge, this is the first time that a precise density demarcation value has been identified for the selection of the different models. We show that excitation transfer processes (and not metastables excitation contributions) are in fact the dominant secondary processes that invalidate the SSC model at densities above $10^{11}\,\mathrm{cm}^{-3}$.

[1] V. A. Godiak, R. B. Piejak, and B. M. Alexandrovich, J. Appl. Phys. **73**, 3657 (1993).
[2] V. A. Godiak, R. B. Piejak, B. M. Alexandrovich, and V. I. Kolobov, Phys. Rev. Lett. **80**, 3264 (1998).
[3] I. D. Sudit and F. F. Chen, Plasma Sources Sci. Technol. **3**, 162 (1994).
[4] E. E. Scime, P. A. Keiter, M. W. Zintl *et al.*, Plasma Sources Sci. Technol. **7**, 186 (1998).
[5] H. Morkoc, S. Strite, G. B. Gao *et al.*, J. Appl. Phys. **76**, 1363 (1994).
[6] R. H. Goulding, F. W. Baity, G. C. Barber *et al.*, Bull. Am. Phys. Soc. **44**, 8 (1999).
[7] F. R. Chang Diaz, R. H. Goulding, R. D. Benson *et al.*, Fusion Technol. **35**, 243 (1999).
[8] S. A. Cohen, B. Berlinger, V. Corso *et al.*, Bull. Am. Phys. Soc. **44**, 8 (1999).
[9] P. A. Keiter, E. E. Scime, and M. M. Balkey, Phys. Plasmas **4**, 2741 (1997).
[10] S. P. Cunningham, in Conf. on Thermonuclear Reactors, Livermore, U.S. Atomic Energy Commission Rep. **279**, 289 (1955).
[11] C. C. Lin and R. M. St. John, Phys. Rev. **128**, 1749 (1962).
[12] R. J. Sovie, Phys. Fluids **7**, 613 (1964).
[13] H. W. Drawin, Z. Naturforsch. A **19**, 1451 (1964).
[14] R. F. De Vries and R. Mewe, Phys. Fluids **9**, 414 (1966).
[15] H. W. Drawin and H. Henning, Z. Naturforsch. A **22**, 587 (1967).
[16] B. J. Eastlund, D. Spero, M. Johnson *et al.*, J. Appl. Phys. **44**, 4930 (1973).
[17] N. J. Brenning, J. Quant. Spectrosc. Radiat. Transf. **24**, 319 (1980).
[18] B. Schweer, G. Mank, A. Pospieszczyk *et al.*, J. Nucl. Mater. **196-198**, 174 (1992).
[19] B. Brosda, Ph. D. Thesis, Ruhr-Universitat, Bochum (1993).
[20] See National Technical Information Service Document No. DE95502158INZ (S. Sasaki, S. Takamura, S. Masuzaki *et al.*, He I Line Intensity Ratios in a Plasma for the Fusion Edge Plasmas NIFS-346, 1995). Copies may be ordered from the National Technical Information Service Springfield, VA 22161.
[21] S. J. Davies, P. D. Morgan, Y. Ul'Haq *et al.*, J. Nucl. Mater. **241-243**, 426 (1997).
[22] Y. Andrew, S. J. Davies, D. Elder *et al.*, J. Nucl. Mater. **266-269**, 1234 (1999).
[23] Y. Andrew and M. G. O'Mullane, Plasma Phys. Controlled Fusion **42**, 301 (2000).
[24] R. W. P. McWhirter, *Plasma Diagnostics* (Academic, New York, 1965), p. 201.
[25] F. J. De Heer, R. Hoekstra, A. E. Kingston, and H. P. Summers, J. Nucl. Fusion (Suppl) **3**, 19 (1992).
[26] See National Technical Information Service Document No. DE96725192INZ (V. P. Shevelko and H. Tawara, Cross Sections for Electron-impact Induced Transitions between Excited States in He-n, n' = 2,3 and 4, NIFS-DATA- 28 1995). Copies may be ordered from the National Technical Information Service Springfield, VA 22161.
[27] R. Denkelmann, S. Maurmann, T. Lokajczyk *et al.*, J. Phys. B **32**, 4635 (1999).
[28] T. Watari, T. Hatori, R. Kumasawa *et al.*, Phys. Fluids **21**, 2076 (1978).
[29] R. W. Boswell, Phys. Lett. A **33**, 457 (1970).
[30] T. Shoji, Y. Sakawa, S. Nakazawa, K. Kadota, and T. T. Sato, Plasma Sources Sci. Technol. **2**, 5 (1993).
[31] K. L. Kline, E. E. Scime, P. A. Keiter, M. M. Balkey, and R. F. Boivin, Phys. Plasmas **6**, 4767 (1999).
[32] P. A. Keiter, E. E. Scime, M. Balkey, R. F. Boivin, J. Kline, and S. Peter Gary, Phys. Plasmas **7**, 779 (2000).
[33] E. E. Scime, P. A. Keiter, M. M. Balkey, R. F. Boivin, J. L. Kline, M. Blackburn, and S. P. Gary, Phys. Plasmas **7**, 2157 (2000).
[34] M. M. Balkey, R. F. Boivin, J. L. Kline, and E. E. Scime, Plasma Sources Sci. Technol. **10**, 284 (2001).
[35] E. E. Scime, R. F. Boivin, J. L. Kline, and M. M. Balkey, Rev. Sci. Instrum. **72**, 1672 (2001).
[36] Oriel Instruments, Instruction Manual, Quartz Tungsten Halogen Lamp Standards of Spectral Irradiance, 250 Long Beach Blvd., P.O. Box 872, Stratford, CT 06497 (1996).
[37] Oriel Instruments, Report of Calibration of One Standard of Spectral Irradiance (250–2400 nm), 250 Long Beach Blvd., P.O. Box 872, Stratford, CT 06497 (1999).
[38] F. F. Chen, *Plasma Diagnostics* (Academic, New York, 1965), p. 113.
[39] J. E. Allen, R. L. Boyd, and P. Reynolds, Proc. Phys. Soc. London, Sect. B **70**, 297 (1957).
[40] W. L. Wiese, M. W. Smith, and B. M. Glennon, Atomic Transitions Probabilities. Vol. 1, National Standard Reference Data System NSRDS-NBS-4 (1966).
[41] P. Zhu and R. W. Boswell, Phys. Fluids B **3**, 869 (1991).
[42] F. F. Chen, Plasma Phys. Controlled Fusion **33**, 339 (1991).
[43] F. F. Chen and C. D. Decker, Plasma Phys. Controlled Fusion **34**, 635 (1992).
[44] A. R. Ellingboe, R. W. Boswell, J. P. Booth, and N. Sadehi, Phys. Plasmas **2**, 1807 (1995).
[45] A. W. Molvik, A. R. Ellingboe, and T. D. Rognlien, Phys. Rev. Lett. **79**, 233 (1997).
[46] R. T. S. Chen and N. Hershkowitz, Phys. Rev. Lett. **80**, 4677 (1998).
[47] F. F. Chen and D. D. Blackwell, Phys. Rev. Lett. **82**, 2677 (1999).
[48] D. D. Blackwell and F. F. Chen, Plasma Sources Sci. Technol. **6**, 569 (1997).
[49] See National Technical Information Service Document No. DE93753246INZ (T. Kato, T. Y. Itikawa, and K. Sakimoto, Compilation of Excitation Cross-sections for He Atoms by Electron Impact, NIFS-DATA-15, 1992). Copies may be ordered from the National Technical Information Service Springfield, VA 22161.
[50] T. Kato and R. K. Janev, Nucl. Fusion Suppl. **3**, 33 (1992).
[51] C. E. Moore, Atomic Energy Levels. Vol. 1, National Standard Reference Data System NSRDS-NBS-1935 (1971).
[52] F. J. De Heer, I. Bray, D. V. Fursa, F. W. Bliek, H. O. Folkerts, and R. Hoekstra, Nucl. Fusion Suppl. **6**, 7 (1996).
[53] J. R. Fuhr and W. L. Weise, *CRC Handbook of Chemistry and Physics*, 74th ed. (CRC Press, Boca Raton, 1994), pp. 10–128.
[54] C. E. Theodosiou, At. Data Nucl. Data Tables **36**, 19 (1987).
[55] T. Holstein, Phys. Rev. **72**, 1212 (1947).
[56] T. Holstein, Phys. Rev. **83**, 1159 (1951).

[57]W. L. Wiese, *Plasma Diagnostics* (Academic, New York, 1965), p. 265.
[58]H. W. Drawin and F. Emard, Beitr. Plasmaphys. **30a**, 143 (1973).
[59]A. C. Mitchell and M. W. Zemansky, *Resonance Radiation and Excited Atoms* (Cambridge University Press, Cambridge, MA, 1971).
[60]R. C. Soulsby, B. R. Kent, M. M. Balkey *et al.*, Bulletin of the APS 42nd Annual Meeting of DPP, p. 331, Quebec, Canada (2000).
[61]J.-H. Kim, S.-M. Yun, and H.-Y. Chang, Phys. Lett. A **221**, 94 (1995).
[62]J.-H. Kim, S.-M. Yun, and H.-Y. Chang, IEEE Trans. Plasma Sci. **24**, 1364 (1996).
[63]Y. Sakawa, N. Koshikawa, and T. Shoji, Appl. Phys. Lett. **69**, 1695 (1996).
[64]S.-M. Yun, J.-H. Kim, and H.-Y. Chang, J. Vac. Sci. Technol. A **15**, 673 (1997).
[65]C. D. Lin, W. R. Johnson, and A. Dalgarno, Phys. Rev. A **15**, 154 (1977).
[66]J. R. Woodworth and H. W. Moos, Phys. Rev. A **12**, 2455 (1975).